Asian Journal of Chemistry; Vol. 37, No. 1 (2025), 112-122

ASIAN JOURNAL OF CHEMISTRY

https://doi.org/10.14233/ajchem.2025.32826

Catalyst-Free Synthesis, *in vitro* Biological Evaluation and *in silico* Molecular Docking Studies on a Series of Tosylurea-linked Heterocyclic Analogues as α-Glucosidase Inhibitors

SIVAKAMI JAYA SEELAN[1], DANUSSHA THARMALINGAM[2], VARSHUTHA SURESH[2], VIVI NG WEI YI[2], YAP ROU XIN[2] and VASUDEVA RAO AVUPATI[3,4,*]

[1]School of Postgraduate Studies, IMU University (Formerly known as International Medical University), 126, Jalan Jalil Perkasa 19, Bukit Jalil, 57000 Kuala Lumpur, Malaysia
[2]School of Pharmacy, IMU University (Formerly known as International Medical University), 126, Jalan Jalil Perkasa 19, Bukit Jalil, 57000 Kuala Lumpur, Malaysia
[3]Department of Pharmaceutical Chemistry, School of Pharmacy, IMU University (Formerly known as International Medical University), 126, Jalan Jalil Perkasa 19, Bukit Jalil, 57000 Kuala Lumpur, Malaysia
[4]Centre of Excellence for Bioactive Molecules & Drug Delivery, Institute for Research, Development & Innovation, IMU University (Formerly known as International Medical University), 126, Jalan Jalil Perkasa 19, Bukit Jalil, 57000 Kuala Lumpur, Malaysia

*Corresponding author: E-mail: vasudevaraoavupati@gmail.com

Received: 2 October 2024; *Accepted*: 6 December 2024; *Published online*: 31 December 2024; AJC-21858

Insulin resistance, caused by hyperglycemia, the leading cause of the global prevalence of type 2 diabetes. According to recent WHO statistics, 422 million people worldwide suffer from diabetes. α-Glucosidase inhibitors are effective in improving the metabolic profile of patients with type 2 diabetes. The introduction of green chemistry into chemical society has led to the rapid establishment of organic synthesis without catalyst. Hence, a series of tosylurea-linked heterocyclic analogues **C1-C9** were synthesized in catalyst-free conditions and their physical (state, colour, melting point) and spectral (FT-IR, ^{1}H NMR, ^{13}C NMR and ESI-HRMS) properties were determined. All compounds were studied *in silico* and *in vitro* experiments to assess their bioactive potential as α-glucosidase inhibitors. The *in silico* molecular docking studies were conducted using Schrödinger Glide software against human α-glucosidase enzyme target (PBD: 3L4W) to identify the virtual binding profile of compounds **C1-C9**, respectively in relative comparison to the co-crystallized clinically approved α-glucosidase inhibitor. The *in vitro* α-glucosidase screening assay was performed to identify the hit molecule among **C1-C9**, the results were compared with a standard drug, voglibose. The observed *in silico* and *in vitro* results were consistent and relatively comparable that identified **C7** as bioactive hit that demonstrated most stable binding properties at the target site. The observed activity of **C7** is primarily due to the synergistic or addition potential of the pharmacophores pyridine and sulfonylurea hybridized into one molecule. The structural analogues of these pharmacophores were earlier proven with potential α-glucosidase inhibitory properties.

Keywords: Catalyst-free synthesis, Tosylurea-linked heterocyclics, Molecular docking studies, α-Glucosidase inhibitors.

INTRODUCTION

The integration of green chemistry in designing alternative synthetic protocols for value-added products or compounds presents a significant challenge to today's organic chemists and researchers [1]. The fundamental challenge for developing a sustainable chemical enterprise will be finding creative ways to minimize human exposure to and the environmental impact of harmful chemicals while enhancing scientific progress [2]. Catalyst-free organic synthesis, a significant component of green chemistry, has rapidly developed and gained widespread use due to its straightforward, low-cost and convenient process for easy separation and purification. Significant catalysts are often expensive and difficult to recycle, resulting in revenue loss and environmental contamination. Therefore, the development and application of catalyst-free organic reactions hold substantial importance and will surely attract the interest of academics; simultaneously, it is expected to benefit the chemical industry and society as a whole [3]. Catalyst-free synthesis may also be a sustainable method in synthetic organic chemistry.

Researchers employ various catalyst-free synthesis methods, including room temperature catalyst-free organic reactions [4], conventional heating catalyst-free organic reactions, microwave irradiation, ultrasound irradiation and ball milling catalyst free organic reactions, among others [5].

Diabetes mellitus (DM) is a chronic metabolic condition characterized by insulin secretion deficiencies or insulin resistance, resulting in hyperglycemia [6]. The progression of DM can bring complications such as heart disease, amputations, kidney issues and neurodegenerative disorders. As per the International Diabetes Federation report, DM poses a substantial global health challenge, affecting 537 million adults worldwide in 2021, with figures anticipated to rise to 783 million by 2045 [7]. The most prevalent forms of diabetes include type 1 DM (T1DM), type 2 DM (T2DM) and gestational DM, with T2DM representing approximately 90% of the cases globally. There are many treatments available for T2DM right now, ranging from pills like biguanides, sulphonylureas and α-glucosidase inhibitors (α-GIs) that lower blood sugar to insulin or glucagon like peptide-1 receptor agonists which are injected [8]. The intestinal brush border contains the digestive enzyme glucosidases. This is an important enzyme that helps break down the glycosidic bonds of disaccharides like maltose and sucrose into their monosaccharide parts, glucose and fructose. This enzymatic activity is pivotal in regulating the availability of glucose after meals and helps to manage postprandial hyperglycemia. Without α-glucosidase action, complex carbohydrates would remain undigested, potentially leading to nutritional deficiencies and disrupted energy metabolism. As a result, α-glucosidase is identified as a primary target enzyme in both the prevention and management of T2DM. In diabetics, α-glucosidase inhibitors (AGIs) are essential for controlling blood glucose levels after meals. They help to maintain normal blood glucose levels by delaying carbohydrate digestion and reducing monosaccharide absorption [9].

The iterative process of drug discovery aims to identify promising therapeutic candidates to treat multifactorial diseases. The drug discovery process included identifying and validating a druggable molecular target, developing bioassays for screening and prioritizing hits, leads and drug-like molecules. After meeting these prerequisites, the drug candidate advances to preclinical development and clinical trial phases (phases I to IV) to establish safety and efficacy in humans and determine potential drug-drug interactions. Phase IV trials culminate in post-marketing surveillance, where the spontaneous reporting of adverse events ensures a continuous assessment of the drug's safety profile. Currently, computer-aided drug design (CADD) is a key part of finding new drugs. A crucial aspect of CADD is docking studies, which evaluate the interactions between ligands and target proteins. Molecular docking emphasizes the binding of a single ligand to a specific target protein, whereas cross-docking focuses on multiple ligands docked to target proteins. Thus, we commonly conduct molecular docking for lead identification, while we perform cross-docking for broad-spectrum drug discovery and assessing protein flexibility. Finding leads is easier with these docking results because they show how proteins and ligands bind, interact and arrange themselves in complexes. Hence, CADD is essential tool to discover new drugs [10]. This study is presented as an extension of the research conducted by medicinal chemists to refine the conditions for different synthetic organic compounds, focusing on the synthesis of a series of tosylurea-linked heterocyclic analogues without the use of catalysts. Based on the literature survey, there is no no report addressing the proposed objectives of this study, highlighting the novelty of this work. Therefore, we designed specifically to synthesize and evaluate *in vitro*-glucosidase inhibitory potential and *in silico* stable binding properties at the target binding site region. Based on our earlier studies, tosylurea is identified as a vital pharmacophore towards α-glucosidase inhibitory potential [11]. Thus, the effect of substituting a heterocyclic ring onto the tosylurea molecule will be explored.

EXPERIMENTAL

All the reagents and chemicals were procured from Sigma-Aldrich, USA, which includes *p*-toluenesulfonyl isocyanate, 3-morpholinopropylamine, 4-aminomorpholine, 2-thiophenemethylamine, 4-(aminomethyl)pyridine, 2-picolyamine, 3-(aminomethyl)-1-methylindole, 2-amino-4,6-dimethoxypyrimidine, 3-aminooxetane, 1-aminohomopiperidine, anhydrous sodium sulphate, acetone, methanol, chloroform and dichloromethane, respectively.

The reaction progress and purity of the synthesized compounds were checked on pre-coated 60 F_{254} silica gel TLC plates (Merck, 0.25 mm) thickness by means of a gradient solvent system with *n*-hexane and ethyl acetate. Fourier transform infrared spectrometer (Shimadzu, Model: MIRAffinity-1S, Japan) used to record the spectra. ^{1}H NMR & ^{13}C NMR spectra recorded on a Varian NMR System (Varian, 500 MHz, USA) using TMS (tetramethylsilane) as an internal standard. Weighing balance (Mettler Toledo, Model: ML204, USA) was used to weigh the chemicals used in the synthetic protocols. The electrospray ionization mass spectra (ESI-MS) were recorded using high-resolution mass spectrometry (HRMS) (Thermo-Scientific, Q Exactive Focus (Orbitrap LC-MS/MS System, USA)). Melting point apparatus (Stuart Scientific, Model: SMP1, U.K.) were determined in the open capillary tubes and are uncorrected. Schrödinger Drug Discovery software and computer hardware facilities were used to perform molecular simulation studies [12].

General procedure for the synthesis of tosylurea-linked heterocyclic analogues (C1-C9): The tosylurea-linked heterocyclic analogues (**C1-C9**) were synthesized by transferring tosylisocyanate (0.015 M) into a conical flask (100 mL) charged with amino heterocycles (0.01 M) in 20 mL of dichloromethane. The reaction mixture was gently stirred at room temperature using a glass rod continuously for 10 min without adding any catalyst. The resulting reaction mixture was stirred using a glass rod for 10-15 min at room temperature till solid amorphous powder precipitated. The beaker containing the crude solid product was covered with parafilm and left to dry at room temperature for 24 h prior to recrystallization. TLC was performed to check the completion of the reaction. A solid white coloured precipitate was observed for all the synthesized compounds **C1-C9**. Following the vacuum filtration of the products with cold methanol and recrystallization was performed using ethanol.

Scheme-I shows the chemical synthetic scheme of compounds **C1-C9**.

4-Methyl-*N*-(oxetan-3-ylcarbamoyl)benzenesulfonamide (C1): Yield: 54.90%; white amorphous powder; m.p.: 152-155 ºC; m.f.: $C_{11}H_{14}N_2O_4S$; Relative molecular mass: 270; FT-IR (ATR, ν_{max} cm^{-1}): 3288.63 (*sec*. amide N-H *str.*), 1707.00 (C=O *str.*), 1558.48 (aromatic C=C *str.*); ^{1}H NMR (500 MHz, DMSO-d_6) δ ppm: 2.36 (s, 3H, Ar-CH_3), 7.38 (d, 2H, *J* = 10 MHz, Ar-H), 7.77 (d, 2H, *J* = 5 MHz, Ar-H), 7.22 (s, 1H, -NH), 4.35 (m, 2H, -CH), 4.60 (m, 3H, -CH); ^{13}C NMR (500 MHz, DMSO-d_6) δ ppm: 151.25, 144.08, 137.74, 129.83, 127.74, 77.43, 44.86, 40.44, 40.28, 40.11, 39.94, 39.77, 39.61, 39.44, 21.47; ESI-HRMS (*m/z*): 271.0746 $[M+H]^+$ (positive-ion mode).

4-Methyl-*N*-((thiophen-2-ylmethyl)carbamoyl)benzenesulfonamide (C2): Yield: 53.96%; white amorphous powder; m.p.: 180-184 ºC; m.f.: $C_{13}H_{14}N_2O_3S_2$; Relative molecular mass: 310; FT-IR (ATR, ν_{max} cm^{-1}): 3319.49 (*sec.* amide N-H *str.*), 1654.92 (C=O *str.*), 1539.20 (aromatic C=C *str.*); ^{1}H NMR

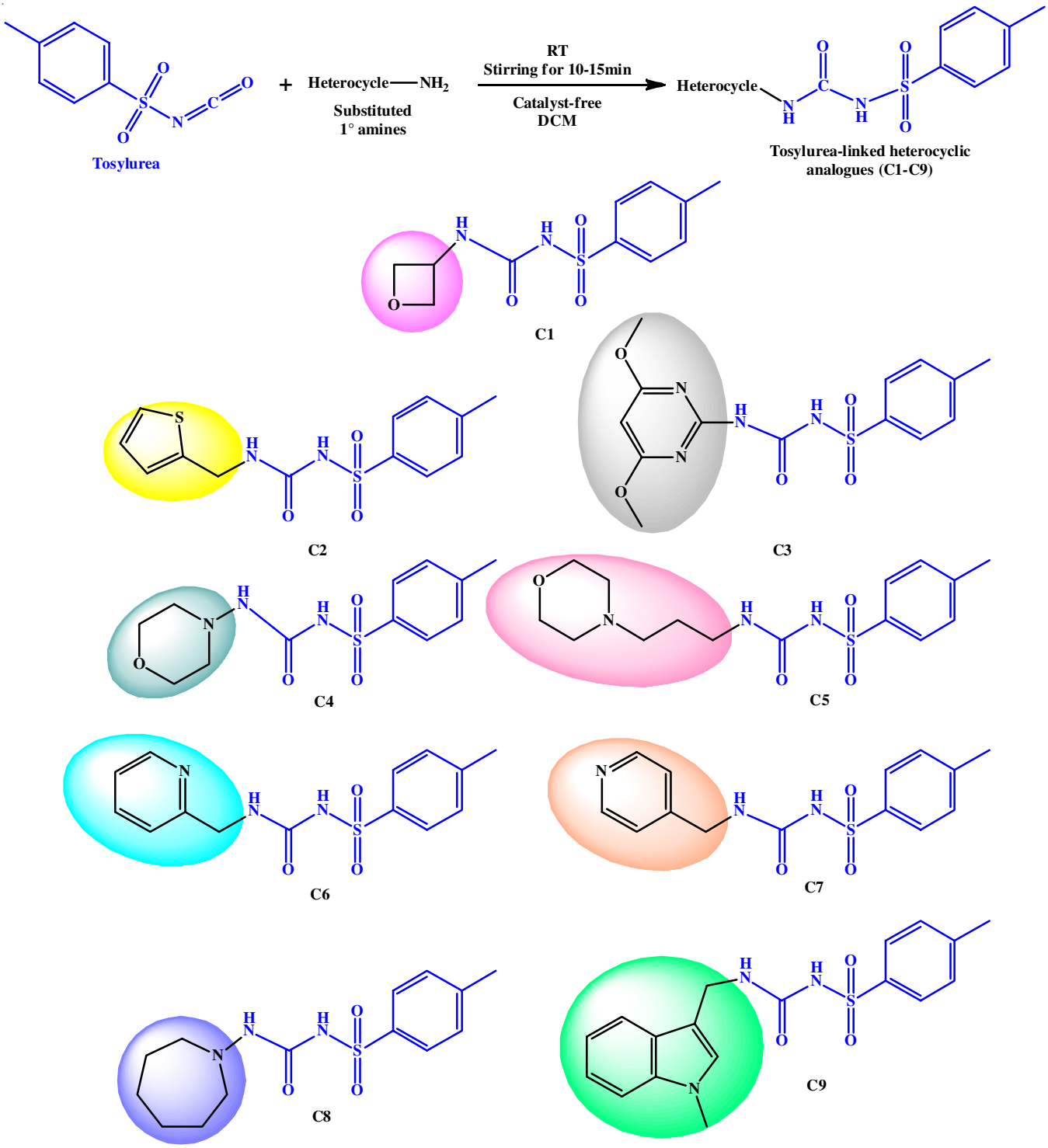

Scheme-I: Synthetic reaction scheme of tosylurea-linked heterocyclic analogues (**C1-C9**)

(500 MHz, DMSO-d_6) δ ppm: 2.37 (s, 3H, Ar-C**H**$_3$), 7.39 (d, 2H, *J* = 10 MHz, Ar-H), 7.78 (d, 2H, *J* = 10 MHz, Ar-H), 7.04 (t, 1H, J_1 = 5 MHz, J_2 = 10 MHz, Ar-H), 7.34 (m, 1H, Ar-H), 6.86 (s, 1H, N**H**), 10.69 (s, 1H, N**H**), 4.30 (d, 2H, *J* = 5 MHz, -C**H**); ^{13}C NMR (500 MHz, DMSO-d_6) δ ppm: 151.73, 144.09, 142.52, 137.76, 129.87, 127.66, 127.08, 125.89, 125.55, 40.45, 40.28, 40.11, 39.95, 39.78, 39.61, 39.44, 38.29, 21.48; ESI-HRMS (*m/z*): 311.0518 $[M+H]^+$ (positive-ion mode).

***N*-((4,6-Dimethoxypyrimidin-2-yl)carbamoyl)-4-methyl-benzenesulfonamide (C3):** Yield: 89.65%; white amorphous powder; m.p.: 176-184 ºC; m.f.: $C_{14}H_{16}N_4O_5S$; Relative molecular mass: 352; FT-IR (ATR, ν_{max} cm^{-1}): 3234.62 (*sec.* amide N-H *str.*), 1697.36 (C=O *str.*), 1570.06 (aromatic C=C *str.*); ^{1}H NMR (500 MHz, DMSO-d_6) δ ppm: 2.49 (s, 3H, Ar-C**H**$_3$), 3.89 (s, 6H, Ar-2 × OC**H**$_3$), 7.43 (d, 2H, *J* = 10 MHz, Ar-H), 7.89 (d, 2H, *J* = 10 MHz, Ar-H), 5.96 (s, 1H, Ar-H), 10.51 (s, 1H, N**H**), 12.55 (s, 1H, N**H**), 4.30 (d, 2H, *J* = 5 MHz, -C**H**); ^{13}C NMR (500 MHz, DMSO-d_6) δ ppm: 172.04, 171.61, 163.15, 156.45, 149.08, 144.91, 142.29, 141.85, 130.04, 129.73, 128.27, 126.05, 84.07, 78.31, 55.04, 53.62, 40.44, 40.27, 40.10, 39.94, 39.77, 39.60, 39.44, 21.52, 21.34; ESI-HRMS (*m/z*): 353.0912 $[M+H]^+$ (positive-ion mode).

4-Methyl-*N*-(morpholinocarbamoyl)benzenesulfonamide (C4): Yield: 17.83%; white amorphous powder; m.p.: 206-208 ºC; m.f.: $C_{12}H_{17}N_3O_4S$; Relative molecular mass: 299; FT-IR (ATR, ν_{max} cm^{-1}): 3244.27 (*sec*. amide N-H *str.*); 1707.00 (C=O *str.*); 1597.06 (aromatic C=C *str.*); ^{1}H NMR (500 MHz, DMSO-d_6) δ ppm: 2.37 (s, 3H, Ar-C**H**$_3$), 7.38 (d, 2H, *J* = 5 MHz, Ar-H), 7.80 (d, 2H, *J* = 5 MHz, Ar-H), 8.29 (s, 1H, N**H**), 10.25 (s, 1H, N**H**), 3.61 (s, 4H, 2 × -C**H**$_2$), 2.67 (s, 4H, 2 × -C**H**$_2$); ^{13}C NMR (500 MHz, DMSO-d_6) δ ppm: 143.95, 137.85, 129.73, 127.87, 66.11, 55.99, 40.45, 40.29, 40.12, 39.95, 39.78, 39.62, 39.45, 21.47; ESI-HRMS (*m/z*): 300.1015 $[M+H]^+$ (positive-ion mode).

4-Methyl-*N*-((3-morpholinopropyl)carbamoyl)benzenesulfinamide (C5): Yield: 32.68%; white amorphous powder; m.p.: 158-161 ºC; m.f.: $C_{15}H_{23}N_3O_3S$; Relative molecular mass: 325; FT-IR (ATR, ν_{max} cm^{-1}): 3213.41 (*sec*. amide N-H *str.*), 1699.29 (C=O *str.*), 1573.91 (aromatic C=C *str.*); ^{1}H NMR (500 MHz, DMSO-d_6) δ ppm: 2.36 (s, 3H, Ar-C**H**$_3$), 1.57 (s, 2H, -C**H**$_2$), 2.26 (s, 2H, -C**H**$_2$), 2.97 (s, 2H, -C**H**$_2$), 7.31 (d, 2H, *J* = 10 MHz, Ar-H), 7.71 (d, 2H, *J* = 10 MHz, Ar-H), 7.75 (d, 4H, *J* = 5 MHz, Ar-H), 7.38 (d, 4H, *J* = 10 MHz, Ar-H), 6.49 (s, 2H, N**H**); ^{13}C NMR (500 MHz, DMSO-d_6) δ ppm: 151.60, 143.44, 138.90, 129.80, 129.38, 127.61, 127.58, 66.11, 55.79, 53.36, 52.79, 40.42, 40.34, 40.25, 40.17, 40.08, 39.92, 39.75, 39.58, 39.41, 37.93, 26.03, 21.44, 21.41; ESI-HRMS (*m/z*): 325.2908 $[M^+]$ (positive-ion mode).

4-Methyl-*N*-((pyridin-3-ylmethyl)carbamoyl)benzenesulfonamide (C6): Yield: 93.58%; white amorphous powder; m.p.: 176-178 ºC; m.f.: $C_{14}H_{15}N_3O_3S$; Relative molecular mass: 305; FT-IR (ATR, ν_{max} cm^{-1}): 3300.20 (*sec.* amide N-H *str.*), 1678.07 (C=O *str.*), 1573.84 (aromatic C=C *str.*); ^{1}H NMR (500 MHz, DMSO-d_6) δ ppm: 2.37 (s, 3H, Ar-C**H**$_3$), 4.26 (d, 2H, *J* = 5 MHz, -C**H**$_2$), 7.39 (d, 2H, *J* = 10 MHz, Ar-H), 7.79 (d, 2H, *J* = 5 MHz, Ar-H), 8.47 (d, 1H, *J* = 5 MHz, Ar-H), 7.71 (m, 1H, Ar-H), 7.25 (m, 1H, Ar-H), 7.15 (m, 1H, Ar-H); ^{13}C NMR (500 MHz, DMSO-d_6) δ ppm: 157.99, 151.97, 149.22, 144.10, 137.78, 137.14, 129.89, 127.67, 122.66, 121.35, 44.85, 40.45, 40.28, 40.11, 39.94, 39.78, 39.61, 39.44, 21.47; ESI-HRMS (*m/z*): 306.0918 $[M+H]^+$ (positive-ion mode).

4-Methyl-*N*-((pyridin-4-ylmethyl)carbamoyl)benzenesulfonamide (C7): Yield: 40.09%; white amorphous powder; m.p.: 158.0-160 ºC; m.f.: $C_{14}H_{15}N_3O_3S$; Relative molecular mass: 305; FT-IR (ATR, ν_{max} cm^{-1}): 3311.78 (*sec.* amide N-H *str.*), 1662.64 (C=O *str.*), 1564.27 (aromatic C=C *str.*); ^{1}H NMR (500 MHz, DMSO-d_6) δ ppm: 2.38 (s, 3H, Ar-C**H**$_3$), 7.40 (d, 2H, *J* = 10 MHz, Ar-H), 7.78 (d, 2H, *J* = 10 MHz, Ar-H), 4.17 (d, 2H, *J* = 5 MHz, -C**H**$_2$), 7.14 (t, 1H, J_1 = 5 MHz, J_2 = 5 MHz, -C**H**), 8.41 (d, 2H, *J* = 5 MHz, Ar-H), 7.07 (d, 2H, *J* = 5 MHz, Ar-H); ^{13}C NMR (500 MHz, DMSO-d_6) δ ppm: 152.19, 149.82, 148.78, 144.15, 137.71, 129.90, 127.67, 122.23, 42.26, 40.44, 40.27, 40.11, 39.94, 39.77, 39.61, 39.44, 21.47; ESI-HRMS (*m/z*): 306.0911 $[M+H]^+$ (positive-ion mode).

***N*-(Azepan-1-ylcarbamoyl)-4-methylbenzenesulfonamide (C8):** Yield: 34.89%; white amorphous powder; m.p.: 160-163 ºC; m.f.: $C_{14}H_{21}N_3O_3S$; Relative molecular mass: 311; FT-IR (ATR, ν_{max} cm^{-1}): 3309.85 (*sec.* amide N-H *str.*), 1697.36 (C=O *str.*), 1558.48 (aromatic C=C *str.*); ^{1}H NMR (500 MHz, DMSO-d_6) δ ppm: 2.37 (s, 3H, Ar-C**H**$_3$), 7.38 (d, 2H, *J* = 5 MHz, Ar-H), 7.80 (d, 2H, *J* = 5 MHz, Ar-H), 2.87 (s, 2H, -C**H**$_2$), 2.69 (s, 2H, -C**H**$_2$), 1.57 (d, 8H, *J* = 45 MHz, 4 × -C**H**$_2$); ^{13}C NMR (500 MHz, DMSO-d_6) δ ppm: 152.52, 143.98, 129.74, 127.83, 58.57, 40.45, 40.38, 40.28, 40.21, 40.12, 39.95, 39.78, 39.62, 39.45, 26.95, 25.48, 21.47; ESI-HRMS (*m/z*): 312.1376 $[M+H]^+$ (positive-ion mode).

4-Methyl-*N*-(((1-methyl-1*H*-indol-3-yl)methyl)carbamoyl)benzenesulfonamide (C9): Yield: 38.57%; Pale orange powder; m.p.: 155-157 ºC; m.f.: $C_{18}H_{19}N_3O_3S$; Relative molecular mass: 357; FT-IR (ATR, ν_{max} cm^{-1}): 3323.35 (*sec.* amide N-H *str.*), 1653.00 (C=O *str.*), 1533.41 (aromatic C=C *str.*); ^{1}H NMR (500 MHz, DMSO-d_6) δ ppm: 2.38 (s, 3H, Ar-CH_3), 7.37 (d, 2H, *J* = 10 MHz, Ar-H), 7.76 (d, 2H, *J* = 5 MHz, Ar-H), 4.27 (d, 2H, *J* = 5 MHz, Ar-H), 3.69 (s, 3H, -CH_3), 2.69 (s, 2H, -CH_2), 7.40 (d, 1H, *J* = 5 MHz, Ar-H), 6.95 (t, 1H, J_1 = 5 MHz, J_2 = 10 MHz, Ar-H), 6.65 (t, 1H, J_1 = 5 MHz, J_2 = 5 MHz, Ar-H), 7.14 (t, 2H, J_1 = 10 MHz, J_2 = 5 MHz, Ar-H); ^{13}C NMR (500 MHz, DMSO-d_6) δ ppm: 151.59, 144.03, 137.77, 137.13, 129.84, 128.54, 127.66, 126.91, 121.75, 119.19, 119.12, 111.58, 110.12, 40.43, 40.27, 40.10, 39.93, 39.77, 39.60, 39.43, 34.90, 32.71, 21.49; ESI-HRMS (*m/z*): 358.1205 $[M+H]^+$ (positive-ion mode).

General procedure for *in vitro* α-glucosidase inhibitor screening: The α-glucosidase inhibitory activity of compounds (**C1-C9**) was evaluated using the *in vitro* α-glucosidase enzymatic kinetics method [13,14]. Initially, 100 mL of phosphate buffer solution (PBS) was prepared using pre-adjusted buffer tablet dissolved using distilled water. The enzyme concentrations (0.8 to 0.0125 U/mL) were prepared in PBS, alongside 4-nitro-phenyl-D-glucopyranoside (pNPG) prepared in PBS (0.8 to 0.0125 mM), in addition test compounds and the standard were also prepared 100 µM concentration in DMSO. A calibration graph constructed ($r \geq 0.999$) plotted for the reaction mixture concentrations enzyme (0.1 U/mL) against substrate

(0.8 to 0.0125 mM) at UV 405 nm. The screening was performed by measuring the absorbances of liberated *p*-nitrophenol (yellow) in sample/blank reaction mixtures at 405 nm. The total microplate well volume of 130 µL that includes control (enzyme-120 µL, phosphate buffer-5 µL, phosphate buffer + substrate-5 µL), reaction control–blank (enzyme-120 µL, phosphate buffer-10 µL), reaction test (enzyme-120 µL, DMSO + test compound- 5 µL, phosphate buffer + substrate-5 µL), reaction solvent blank (enzyme: 120 µL, DMSO: 5 µL, phosphate buffer + substrate-5 µL), reaction standard (enzyme-120 µL, phosphate buffer + substrate-5 µL, DMSO + voglibose-5 µL (100 µM to 0.5 µM). All the solutions were subjected to enzyme kinetics for 20 min to measure the absorbance. The percentage (%) enzyme inhibition calculated using the following formula: Enzyme inhibition (%) = (1-Absorbance$_{\text{test compound}}$-Absorbance $_{\text{solvent blank}}$/Absorbance$_{\text{control}}$-Absorbance$_{\text{control blank}}$) × 100.

Statistical analysis was carried out using Microsoft Excel.

***in silico* Molecular docking studies**

Target selection: In first step, the human α-glucosidases were searched for the 3D structures database of the National Centre for Biotechnology Information (NCBI). Screening a list of protein Data Bank (PDB) entries (3D structure) fulfilling the given search criteria through the validation criterion [15].

Target validation: The PDB IDs were then validated based on the specific criteria. The requirements included the absence of protein breaks on the 2D view of the 3D protein in PDBsum (https://www.ebi.ac.uk/thornton-srv/databases/pdbsum). If breaks were present without interfering binding site residues, the target was considered. Next, the target was required to fulfill the Ramachandran statical standards, with residues in the generously allowed regions (0-2%) and disallowed regions (0%) and co-crystallized with a standard α-GI to identify a reliable binding site for docking simulations [16].

Target preparation: The integrated option on Schrödinger Software Protein Preparation Workflow (Beta)™ was used to automatically import the selected PDB ID into the workspace. Default settings under preparation workflow (pre-processing, optimizing H-bond assignments and cleaning up), diagnostics and substructures were retained [17].

Molecular modelling: ChemDraw software was used to draw the 2D structure of standard AGIs and experimental compounds (**C1-C9**). The SMILES codes of the 2D structures were then generated for Maestro software to be converted into the 3D structures using integrated options.

Molecular energy minimization: The 3D ligands were subjected to energy minimization using Force Field Orthogonal Partial Least Squares of Schrödinger Software LigPrep™. The default settings were adjusted to neutralize and generate all combinations with one outcome to obtain the most stable ligands saved as a database file.

Binding site generation: Schrödinger Software Glide™ was used to generate the binding site on the prepared target with default configurations for site constraints, rotatable groups and excluded volumes. The target was configured using the "pick to identify the ligand" option to visualize the atoms of the co-crystallized α-GI and select a highlighted atom to form the binding site.

Molecular docking: Schrödinger Software Glide™ was used for molecular docking and consensus scoring. The binding site file of the target was selected as the input for the receptor grid and the ligand database file was uploaded as an SD file. Docking runs were performed with three methods, high throughput virtual screening (HTVS), standard precision (SP) and extra precision (XP), by selection under settings. Each method with distinct scoring and pose selection specifications was employed in parallel to provide a thorough analysis and assess the reproducibility of interactions of test compounds with the target [18].

Validation of molecular docking: The docking protocols were validated by redocking the co-crystallized ligand into the active site of the target. The re-docked complex was superimposed onto the original co-crystallized structure and the root mean square deviation (RMSD) was calculated. RMSD values between 0 Å to 3 Å indicated successful docking, with minimal deviation from the actual co-crystallized complex.

Analysis of docking results: Docking outcomes including docking scores and ligand interaction diagrams (LIDs) from molecular docking studies were generated from Schrödinger Software Maestro™ to determine virtual binding properties. Docking scores of test compounds and standard α-GI, corresponding to its target across all docking methods, were exported into Microsoft Excel for comparative analysis. The LIDs of test compounds provided insights into the interactions with the binding site amino acids of each method. Key amino acids essential for α-glucosidase inhibition were identified by analyzing LigPlot diagrams (2D representations of 3D protein-ligand complexes determined by X-ray crystallography) of the standard α-GI (miglitol) co-crystallized with the selected target.

RESULTS AND DISCUSSION

The chemical structures of the tosylurea-linked heterocyclic analogues **C1-C9** were established through systematic analysis of data from physico-chemical and spectral analysis and found the data to be consistent with the predicted structures based on the conventional reaction-based product formation. The ESI-HRMS positive-mode spectrum of **C1** revealed a pseudo-molecular ion at 271.0746 mass-to-charge ration (*m/z*) as $[M+H]^+$ ion which is consistent with its calculated relative molecular mass of **C1**. Likewise, **C2** at 311.0518 *m/z*, **C3** at 353.0912 *m/z*, **C4** at 300.1015 *m/z*, **C5** at 342.1491 *m/z*, **C6** at 306.0918 *m/z*, **C7** at 306.0911 *m/z*, **C8** at 312.1376 *m/z* and **C9** at 358.1205 *m/z*, respectively. All the compounds exhibited a similar pattern of adduct formation under ESI-positive ionization analysis. The protonated form of all compounds was found to be the base peak with greater relative abundance. The characteristic vibrational bands were observed at various frequencies on the FT-IR spectrum of compounds **C1-C9** consistent with the functional groups secondary amino, carbonyl and alkenyl stretches within the ranges 3213.41-3323.35, 1653.00-1707.00 and 1533.41-1597.06 cm^{-1}, respectively.

The 500 MHz ^{1}H NMR spectrum of compounds **C1-C9** in DMSO-d_6 with TMS as an internal standard exposed a set of different types of protons. The presence of a singlet signal within the range of δ 2.36-2.49 ppm revealed the integration

of three protons, which is consistent with the characteristic range of aromatic methyl protons of an organic compound, observed among all compounds **C1**–**C9**. The presence of two doublet signals, one within the range of δ 7.31-7.89 ppm and the other within the range of δ 7.38-8.41 ppm, revealed the integration of two protons per doublet relatively with the corresponding coupling constants J = 10 MHz and J = 5 MHz, respectively, that are consistent with the characteristic range of four aromatic protons of phenyl ring of the tosyl moiety organic compound, observed among all compounds **C1-C9**. The presence of a singlet signal within the range δ 6.49-12.55 ppm revealed the integration of one proton, which is approximated as an amide proton by its peak characteristic, observed among all compounds **C1**–**C9**, except for the secondary amido proton due to the deuterium water exchange. Besides the above characteristic peaks, there are additional aromatic peaks observed for **C1-C9** within the range of 6.86-8.47 ppm based on its heterocycle connected, such as in case of **C1**, the presence of multiplet signals at δ 4.35 ppm and δ 4.60 ppm revealed the integration of two and three protons, respectively, which were consistent with the characteristic range of oxetane ring protons. Similarly, in case of **C2**, The presence of a doublet signal at δ 4.30 ppm with the coupling constant J equal to 5 MHz revealed the integration of two equivalent protons, which were consistent with the characteristic range of methylene protons of an organic compound. The presence of multiplet signals at δ 7.34 ppm revealed the integration of one proton, which is consistent with the characteristic range of aromatic proton of substituted thiophene. The presence of a triplet signal at δ 7.04 ppm revealed the integration of one proton with the corresponding coupling constant J values (J_1 = 5 MHz and J_2 = 10 MHz), which is consistent with the characteristic range of aromatic proton of substituted thiophene. Likewise, **C3** also exhibited multiplet signals at δ 5.96 ppm, revealing the integration of one proton, which is consistent with the characteristic range of aromatic proton of the pyrimidine heterocyclic ring. Equally, **C4** displayed two singlet signals, one at δ 3.61 ppm and the other at δ 2.67, which revealed the integration of four protons each in a total of eight protons, which is consistent with the characteristic range of heterocyclic ring methylene equivalent protons. Alike **C5** showed the presence of three singlet signals, one at δ 1.57, 2.26 and 2.97 ppm, revealing the integration of two protons each in a total of six protons, which is consistent with the characteristic range of aliphatic methylene equivalent protons. The presence of two doublet signals, one at δ 7.75 ppm and the other one at δ 7.38 ppm, revealed the integration of two protons per doublet relatively with the corresponding coupling constants J = 5 MHz and J = 10 MHz, respectively, that are consistent with the characteristic range of eight aromatic protons of an organic heterocyclic morpholine ring of the compound. Similarly, **C6** demonstrated the presence of three multiplet signals at δ 7.71, 7.25 and 7.15 ppm, revealing the integration of three protons, one for each signal consistent with the characteristic range of aromatic proton of an organic compound. The presence of one doublet signal at δ 4.26 ppm revealed the integration of two protons with the corresponding coupling constant J = 5 MHz, which is consistent with the characteristic range of methylene protons of an organic compound. In **C7**, the presence of a triplet signal at δ 7.14 ppm revealed the integration of one proton with the corresponding coupling constant J values (J_1 = 5 MHz and J_2 = 5 MHz), which is consistent with the characteristic range of the methine proton of an organic compound. The presence of one doublet signal at δ 8.41 ppm revealed the integration of two protons with the corresponding coupling constant J = 5 MHz is consistent with the aromatic protons of an organic compound. The presence of one doublet signal at δ 7.07 ppm revealed the integration of two protons with the corresponding coupling constant J = 5 MHz is also consistent with the characteristic range of aromatic protons of an organic compound. The presence of one doublet signal at δ 4.17 ppm revealed the integration of two protons with the corresponding coupling constant J = 5 MHz that is consistent with the characteristic range of methylene protons of an organic compound. As observed in **C8**, the presence of two singlet signals, one at δ 2.87 ppm and the other one at δ 2.69 ppm, revealed the integration of two protons per doublet relatively with the corresponding coupling constants J = 5 MHz and J = 5 MHz, respectively, are also consistent with the characteristic range of four heterocyclic protons of an organic compound. The presence of one doublet signal at δ 1.57 ppm revealed the integration of eight protons with the corresponding coupling constant J = 45 MHz and consistent with the characteristic range of octane heterocyclic compound protons. Finally, **C9** showed the presence of a singlet signal at δ 3.69 ppm revealing the integration of three protons and confirmed the characteristic range of N-methyl protons of a substituted indole moiety. The presence of a singlet signal at δ 2.69 ppm revealed the integration of two protons and confirmed the characteristic range of methylene protons of the substituted indole moiety. The presence of a triplet signal at δ 6.65 ppm revealed the integration of one proton with the corresponding coupling constant J values (J_1 = 5 MHz and J_2 = 5 MHz). The presence of a triplet signal at δ 6.95 ppm revealed the integration of one proton with the corresponding coupling constant J values (J_1 = 5 MHz and J_2 = 10 MHz), which is consistent with the characteristic range of aromatic proton of the substituted indole moiety. The presence of a triplet signal at δ 7.14 ppm revealed the integration of one proton with the corresponding coupling constant J values (J_1 = 10 MHz and J_2 = 5 MHz), confirmed the characteristic range of aromatic proton of the substituted indole moiety.

In ^{13}C NMR spectrum of compound **C1**, the presence of signals at chemical shifts δ 151.25 ppm, δ 21.47 ppm, δ 137.74-127.74 ppm and δ 77.43-40.44 ppm revealed the characteristic presence of a carbonyl (C=O), methyl (aromatic methyl), aromatic and carbocyclic ring carbons, respectively. Similarly, in compound **C2**, the chemical shifts at δ 151.73 ppm, δ 21.48 ppm, δ 137.76-127.08 ppm and δ 40.45 ppm also revealed the characteristic presence of a carbonyl (C=O), methyl (aromatic methyl), aromatic and methylene chain carbon, respectively. In compound **C3**, the presence of signals at chemical shifts δ 156.45 ppm, δ 21.52 ppm, δ 144.01-126.05 ppm and δ 172.04-171.61, 149.08 ppm revealed the presence of a carbonyl (C=O), methyl (aromatic methyl), aromatic and pyrimidine ring carbon atoms, respectively. In addition, there is a specific presence of

methoxyl carbons on the ring system observed at δ 55.04 and 53.62 ppm. In compound **C4**, the chemical shifts δ 143.95 ppm, δ 21.47 ppm, δ 137.85-127.87 ppm and δ 55.99, 66.11 ppm revealed the characteristic presence of carbonyl (C=O), methyl (aromatic methyl), aromatic and morpholine ring carbon atoms. In compound **C5**, the chemical shifts at δ 151.60 ppm, δ 21.44 ppm, δ 138.90-127.58 ppm and δ 55.79, 66.11 ppm revealed the presence of carbonyl (C=O), methyl (aromatic methyl), aromatic and morpholine ring carbon atoms. In compound **C9**, the chemical shifts at δ 151.59 ppm, δ 21.49 ppm, δ 137.77-127.66 ppm and δ 126.91, 121.75, 119.19, 119.12, 111.58, 110.12 and 39.93 ppm revealed the characteristic presence of carbonyl (C=O), methyl (aromatic methyl), aromatic and indole ring carbon atoms, respectively. The above data confirms the theoretical backbone of the carbon atoms connected in the chemical structure of compounds **C1-C9**.

***In vitro* screening:** The α-glucosidase inhibitory activity of the synthesized tosylurea-linked heterocyclic analogues **C1-C9**, demonstrated its bioactivity order as: **C7** (3-pyridine 18.2613%) > **C8** (hexahydro-azepine 17.0786%) > **C4** (morpholine 16.6165%) > **C2** (thiophene 16.2127%) > **C6** (2-pyridine 16.1202%) > **C9** (indole(N-methyl) 10.0692%) > **C5** (morpholine(N-ethyl) 9.1904%) > **C1** (oxetane 5.7741%) > **C3** (pyrimidine 5.2498%). Among the compounds, **C7** was found to be the most active, which further could be analyzed for the determination of IC_{50} value. The structure-activity relationships (SARs) analysis was performed based on the chemical and structural features of a series of nine compounds **C1-C9** with their corresponding % inhibition of α-glucosidase enzyme activity shown in Fig. 1. The assessment focuses on various parameters such as type of heterocycle, size of heterocycle, number of heteroatoms, aromaticity of the heterocycle, substituent on the heterocycle, type and number of substituents, respectively as shown in Table-1.

Present study of heterocycles revealed that the several structural factors influence their reactivity and enzyme interaction. The type of heterocycle plays a crucial role for instance, **C1** (oxetane) is a non-aromatic 4-membered ring with oxygen exhibits low inhibition (5.77%), while **C2** (thiophene), 5-membered aromatic ring with sulfur atom, shows moderate inhibition (16.21%) due to its stability. **C3** (pyrimidine), 6-membered ring containing two nitrogen atoms, has an electron-releasing substituent but still demonstrates low inhibition (5.25%). In contrast, **C4** and **C5** (morpholine), both 6-membered rings with oxygen and nitrogen, show varied inhibition; **C4**, being non-aromatic, has higher inhibition (16.62%) compared to **C5** (9.19%), which

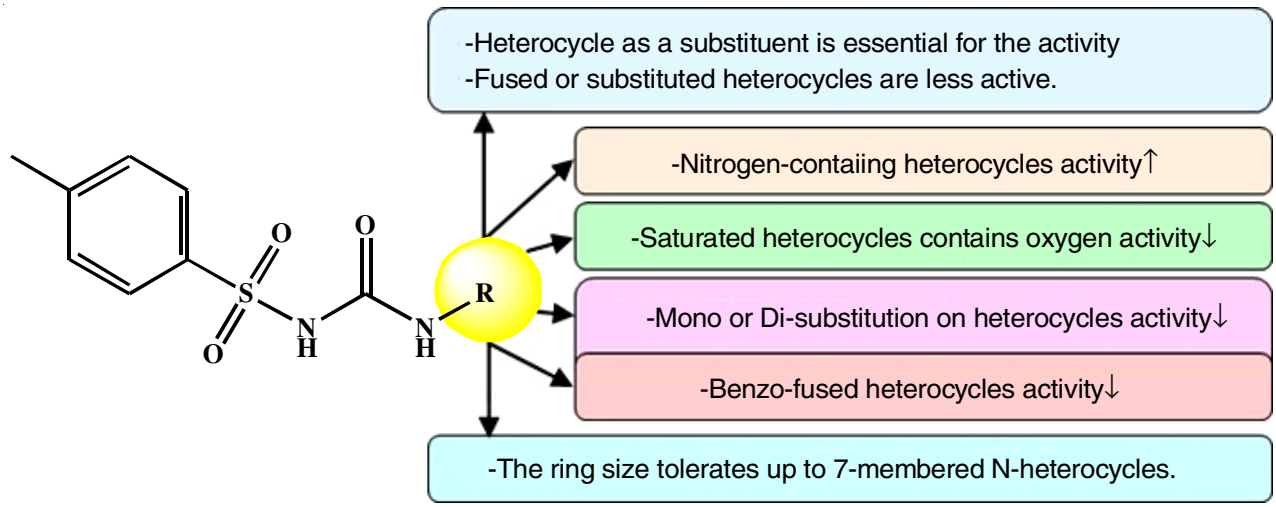

Fig. 1. Structure-activity relationship (SAR) of tosylurea-linked heterocyclic analogues as α-glucosidase inhibitors

TABLE-1
PERCENTAGE INHIBITION OF THE α-GLUCOSIDASE ENZYME ACTIVITY DATA OF COMPOUNDS **C1-C9**

Code	Heterocycle type	Ring size	Type of heteroatom/ Number	Aromaticity	Substituent	Type of substituents/ Number	Inhibition (%)
C1	Oxetane	4-Membered	Oxygen/1	Non-aromatic	0	0	5.77
C2	Thiophene	5-Membered	Sulfur/1	Aromatic	0	0	16.21
C3	Pyrimidine	6-Membered	Nitrogen/2	Aromatic	3,5-Dimethoxyl	Electron-releasing/2	5.24
C4	Morpholine	6-Membered	Oxygen/1 and Nitrogen/1	Non-aromatic	0	0	16.61
C5	Morpholine	6-Membered	Oxygen/1 and Nitrogen/1	Non-aromatic	N-Ethyl	Electron-releasing/1	9.19
C6	2-Pyridine	6-Membered	Nitrogen/1	Aromatic	*ortho*-isomer	0	16.12
C7	3-Pyridine	6-Membered	Nitrogen/1	Aromatic	*para*-isomer	0	18.26
C8	Hexahydro-azepine	7-Membered	Nitrogen/1	Non-aromatic	0	0	17.07
C9	Indole	Benzo-fused-5-Membered	Nitrogen/1	Aromatic	N-methyl	Electron-releasing/1	10.06
			Voglibose				45.01

has a substituent. The 6-membered nitrogen heterocycles **C6** and **C7** differ in inhibition levels, with **C7** (*para*-isomer) showing the highest at 18.26%. The larger 7-membered ring **C8** (hexahydroazepine) also exhibits significant inhibition (17.08%), demonstrating that size can enhance enzyme interaction. The size of the heterocycle affects spatial arrangement and steric effects, with 4-membered rings showing limited steric hindrance and lower inhibition, while 6-membered rings generally provide higher inhibition, particularly when aromatic. The number of heteroatoms is another critical factor; compounds with more heteroatoms, like **C4** and **C5**, tend to show higher inhibition due to enhanced enzyme interactions, while those with only one heteroatom typically exhibit lower inhibition, with **C7** being an exception. Aromaticity significantly impacts stability and reactivity, with aromatic compounds like **C2**, **C3**, **C6**, **C7** and **C9** generally showing higher inhibition percentages; **C7** is the most potent. Non-aromatic compounds, such as **C1**, **C4**, **C5** and **C8**, usually display lower inhibition levels. Additionally, the presence and type of substituents play a vital role; electron-releasing substituents can lead to varied inhibition results, as observed in **C5**. Overall, the measure of % inhibition serves as a primary outcome, highlighting that **C3** (5.25%) and **C1** (5.77%) show minimal activity, while compounds like **C2** (16.21%), **C4** (16.62%) and especially **C7** (18.26%) indicate strong potential for further investigation into enzyme interaction mechanisms.

***In silico* studies:** Initially, the primary search for 3D structures of α-glucosidase in NCBI, 217548 protein entries were selected. Further, an animal species filter was applied, resulting in 9035 entries, which were narrowed down to 118 human taxon entries. The entries with PDB IDs were subjected to the selection and validation process. According to the observations, 3L4W was selected for the molecular docking studies using energy minimized ligands **C1-C9**. The docking protocols were found to be reliable with an ability to reproduce crystallographic binding orientation (RMSD < 1) of the co-crystallized ligand Miglitol as shown in Fig. 2.

The relative comparison of three docking outputs (HTVS, SP and XP) resulted in the identification of the virtual hits were ranked in the order of their ligand stability; the top three ligands of each protocol are shown in Table-2. Based on the results, a re-ranking analysis was performed to identify more specific ligands. Based on their reproducibility of binding energy (docking score), which ligands shown across several docking techniques, shown in Table-3, the ligand to be re-ranked ranked highest. The standard of the docking methods was established as XP > SP > HTVS and the same standards was applied to shortlist the ligands for re-ranking. Subsequently, the hit priori-

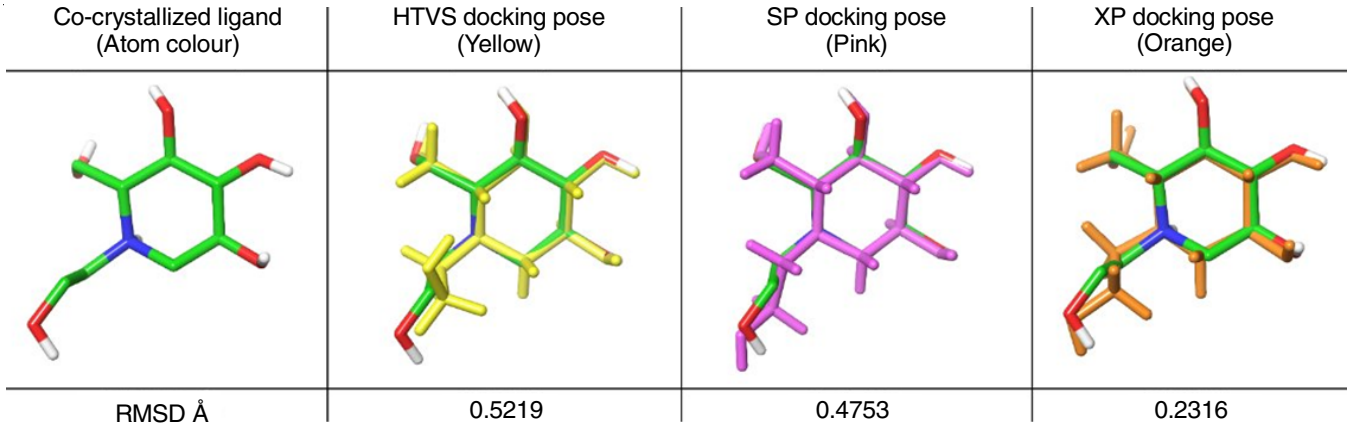

Fig. 2. Superimposed ligand conformations (native pose *versus* predicted pose) predicted by molecular docking protocols

TABLE-2
MOLECULAR DOCKING BASED VIRTUAL SCREENING RESULTS OF **C1-C9** AT THE 3L4W TARGET BINDING SITE REGION

Order of ligand stability	Virtual screening hits against 3L4W					
	HTVS docking		SP docking		XP docking	
	Ligand	Docking score (kcal/mol)	Ligand	Docking score (kcal/mol)	Ligand	Docking score (kcal/mol)
Rank 1	**C2**	-5.16	**C7**	-5.682	**C7**	-5.407
Rank 2	**C1**	-4.924	**C2**	-5.655	**C1**	-4.53
Rank 3	**C4**	-4.619	**C6**	-5.426	**C5**	-4.383

TABLE-3
LIGAND BINDING INTERACTION-BASED PRIORITIZATION OF **C1-C9** AT THE 3L4W TARGET BINDING SITE REGION

Order of Re-ranked ligands	Ligand	Hydrogen bonding interactions 1_3L4W (Binding site residue: Number of hydrogen bonds)		
		HTVS docking	SP docking	XP docking
Re-Rank 1	**C7**	Asp542: 2	Arg526: 1; Asp542: 2	Asp542: 2; Hie600: 1
Re-Rank 2	**C2**	Arg526: 1; Asp542: 1	Arg526: 1; Asp542: 2	Asp542: 2
Re-Rank 3	**C1**	Asp203: 2; Thr205: 1	Asp542: 1; Tyr605: 1	Asp542: 2; Tyr605: 1

tization process was applied to the re-ranked set of ligands. The guidelines were established logically, prioritizing the total count of hydrogen bond-forming amino acids produced by the ligand in relation to the crystallographic binding interactions. The successful ligand was designated as a virtual hit molecule, with **C7** being the prioritized molecule based on the crystallographic binding interaction profile of miglitol within the target binding area of the human α-glucosidase enzyme (PDB ID: 3L4W), as shown in Table-4.

Ligplot interaction profile was studied for the target protein 3L4W in which miglitol is co-crystallized with the α-glucosidase drug target protein (PDB ID: 3L4W). The ligand exhibited selective binding profile in the binding site, consisting of 13 amino acids such as Tyr299, Asp327, Ile328, Ile364, Trp406, Trp441, Asp443, Met444, Arg526, Trp539, Asp542, Phe575 and His600, respectively. Among the residues, 4 amino acids formed six hydrogen bonding interactions, which include Asp327(2), Arg526(1), Asp542(1), His600(2). These hydrogen bond forming amino acids are very crucial to possess α-glucosidase inhibitory properties, therefore, the similar observations were proposed to be re-produced using molecular docking simulation protocol so as to complement the experimental observation using computational algorithms. A close examination into the docking simulations results revealed that the amino acids such as Asp327(2), Arg526(1), Asp542(1), His600 (2) which were forming part of the hydrogen bonding interactions formed at the simulated binding site region (HTVS, SP, XP docking results as shown in Fig. 3) are consistently reproduced similar to the observations reported in the experimental studies. Finally, the data has proven the proposed hypothesis was logically validated using an established docking protocol.

The prioritized hit **C7** revealed characteristic hydrogen bonding interactions with crystallographic amino acids that were forming part of ligand binding interactions displayed by the co-crystallized α-glucosidase inhibitor (miglitol), which includes Asp327, Arg526, Asp542 and His600, respectively as shown in Fig. 4 as well as their 3D binding poses were shown in Fig. 5 [19]. The aspartate residues (Asp327 and Asp542) also play a vital role in the formation of polar interactions with the sugar for the catalytic mechanism [20]. This observation was also supported in X-ray crystallographic studies performed using acarbose [21]. Asp542 acts as the catalytic nucleophile and Asp327 is involved in stabilizing the transition state during the hydrolysis reaction. In addition, Arg526 and His600 are crucial for substrate stabilization within the active site. Arg526 and His600 form multiple hydrogen bonds with the substrate, which helps in substrate positioning and binding for catalysis [22]. Studies have shown that inversion or mutation of these

TABLE-4
RELATIVE COMPARISON OF THE STABLE BINDING PROFILE OF HIT MOLECULE **C7** WITH CO-CRYSTALLIZED LIGAND MIGLITOL

Docking method	Docking score (kcal/mol)		Binding interactions	
	Miglitol	**C7**	Miglitol	**C7**
XP	-7.093	-5.407	Asp327: 2; Arg526: 1; Asp542: 1; His600: 2	Asp542: 2; Hie600: 1
SP	-7.19	-5.682		Arg526: 1; Asp542: 2
HTVS	-7.082	-3.765		Asp542: 2

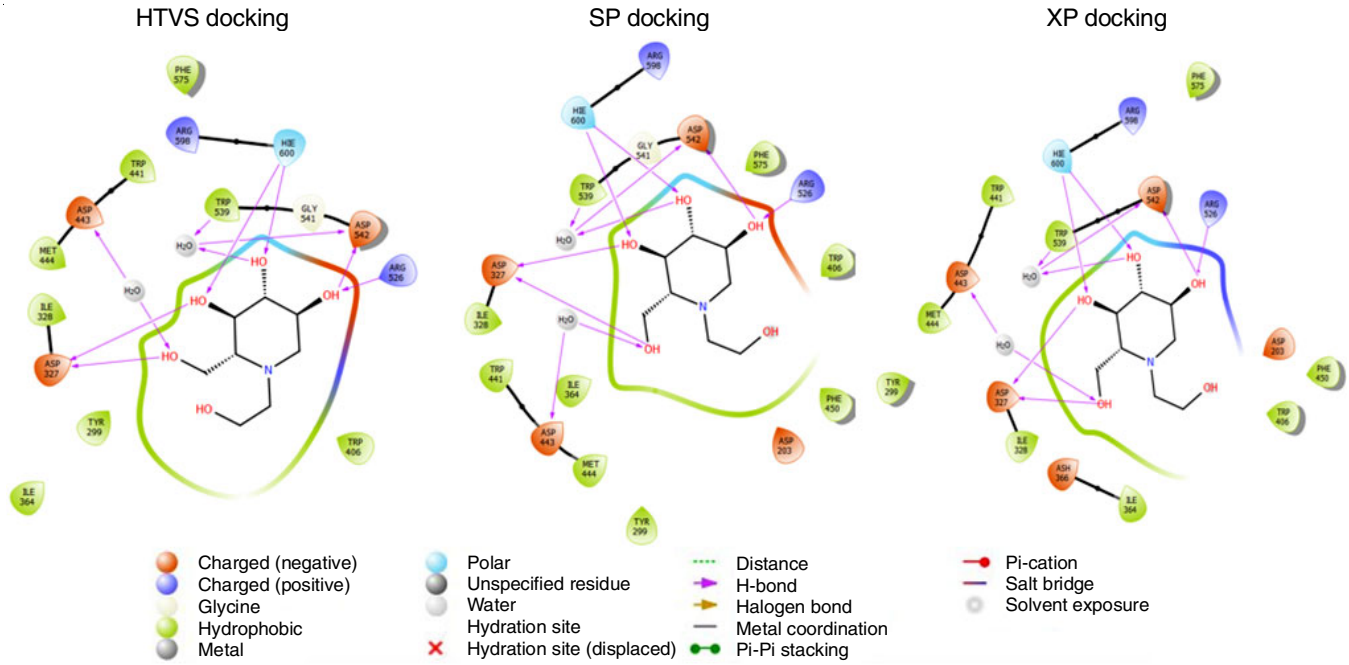

Fig. 3. Ligand-interaction diagrams of Miglitol at the target binding site of human α-glucosidase (PDB ID: 3L4W) in HTVS, XP and SP docking modes

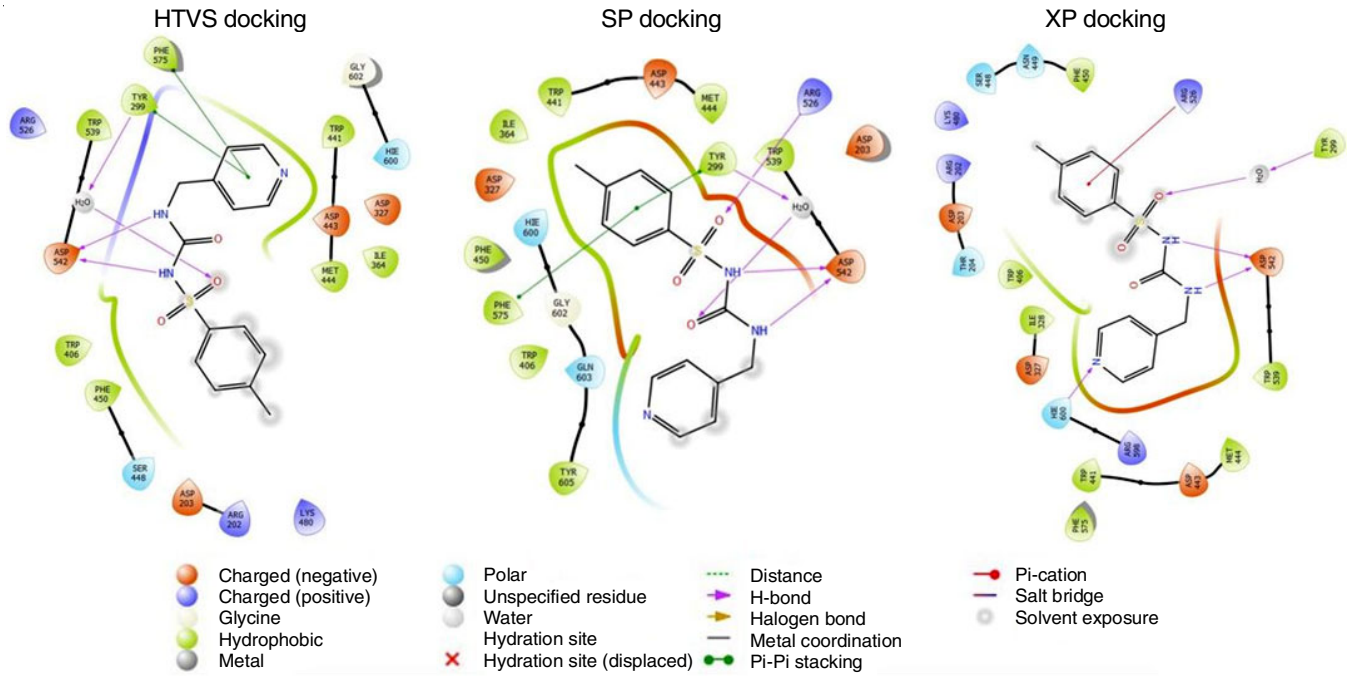

Fig. 4. Ligand-interaction diagrams of **C7** at the target binding site of human α-glucosidase (PDB ID: 3L4W) in HTVS, XP and SP docking modes

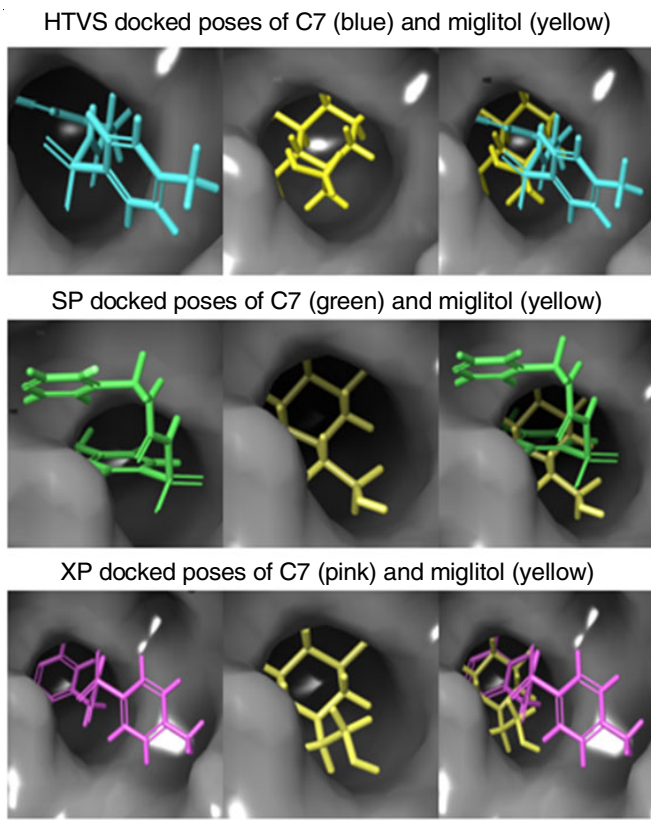

Fig. 5. 3D binding poses of **C7** and miglitol at the target binding site of human a-glucosidase (PDB ID: 3L4W) in various docking modes

residues (Asp327, Arg526, Asp542 and His600) significantly inhibits α-glucose enzyme activity [23]. Based on another mechanistic study, binding interaction with all catalytic residues Asp327, Arg526, Asp542 and His600 is hihgly crucial to controlling the α-glucosidase enzyme activity [24]. In this study, pyridine heterocycle substitution in the tosylurea moiety distinctly contributed to the formation of a hydrogen bond interaction with His600, which is a vital amino acid for the substrate stabilization in the active of human α-glucosidase activity. The tosylurea, which was earlier identified as a potential pharmacophore for human α-glucosidase inhibition, formed hydrogen bonding with other catalytic amino acids Asp327, Arg526 and Asp542 due to its polar nature of sulfonyl (S=O), N1 (NH) of sulfonylurea (NH) and N3 (NH) of sulfonylurea, respectively.

Conclusion

The present investigation determined whether tosylurea-linked heterocyclic analogs may inhibit the activity of α-glucosidase. Thus, a series of tosylurea-linked heterocycles (**C1**–**C9**) was design, synthesized and a systematic approach to investigate their *in vitro* α-glucosidase inhibitory properties and *in silico* binding profile using molecular docking studies (HTVS, SP and XP) at the human target binding site region (PDB ID: 3L4W). The α-glucosidase target was selected based on the co-crystallized ligand-binding interactions with miglitol. Results showed that **C7** has stable binding properties at the target binding site region of 3L4W but is not superior to miglitol (a clinically used drug). Interestingly, **C7** has also been found to be most potent among **C1-C9** tested *in vitro*. The relatively comparable results obtained *in vitro* and *in silico* provided deeper insight into the role of molecular docking accuracy in predicting the prospective ligands to be carried forward to the experimental studies. Therefore, this established docking protocol with 3L4W could be used as a virtual screening tool for a large chemical library as novel α-glucosidase inhibitors.

ACKNOWLEDGEMENTS

The authors are highly grateful to the IMU University Vice Chancellor, Dean, School of Pharmacy, Dean, School of Post-graduate Studies, Director and Deputy Directors of Institute for Research, Development & Innovation (IRDI) for providing the facilities to complete the final year research projects. This research was funded by IMU University Joint-Committee on Research & Ethics, Project IDs No. MSc in Molecular Medicine: MMM I-2021(10) and B Pharm (H): BP I-01-2024(17).

CONFLICT OF INTEREST

The authors declare that there is no conflict of interests regarding the publication of this article.

REFERENCES

1. A. Sarkar, S. Santra, S. Kundu, A. Hajra, G.V. Zyryanov, O.N. Chupakhin, V.N. Charushin and A. Majee, *Green Chem.*, **18**, 4475 (2016); https://doi.org/10.1039/C6GC01279E
2. M.B. Gawande, V.D.B. Bonifácio, R. Luque, P.S. Brancoa and R.S. Varma, *Chem. Soc. Rev.*, **42**, 5522 (2013); https://doi.org/10.1039/C3CS60025D
3. G. Brahmachari and B. Banerjee, *Curr. Green Chem.*, **2**, 274 (2015); https://doi.org/10.2174/2213346102666150218195142
4. B. Banerjee, *Ultrason. Sonochem.*, **35A**, 1 (2017); https://doi.org/10.1016/j.ultsonch.2016.09.023
5. M. Tavakolian and M. Hosseini-Sarvari, *ACS Sustain. Chem.& Eng.*, **9**, 4296 (2021); https://doi.org/10.1021/acssuschemeng.0c06657
6. A.K.D.B.A. Kamar, L.J. Yin, C.T. Liang, G.T. Fung and V.R. Avupati, Med. Drug Discov., 15, 100131 (2022); https://doi.org/10.1016/j.medidd.2022.100131
7. M. Roden, K.F. Petersen and G.I. Shulman, Insulin Resistance in Type 2 Diabetes, Textbook of Diabetes, Wiley pp. 238-249 (2024).
8. D.L.S. Nori, K.V.V.V. Satyanarayan, V.R. Avupati, B.K. Bugata and S. Yenupuri, *Eur. J. Chem.*, **5**, 144 (2014); https://doi.org/10.5155/eurjchem.5.1.144-149.925
9. X.R. Mong, V.R. Avupati, H. Husniza and K.A. Qusay, *Res. J. Chem. Environ.*, **25**, 1 (2021); https://doi.org/10.25303/2510rjce001006
10. Q.J. Wong, Z.H. Low, Z.Y. Chan and V.R. Avupati, *Data Brief*, **55**, 110618 (2024); https://doi.org/10.1016/j.dib.2024.110618
11. A. Harunani, B.C.S. Chua, J.S. Cheong, J.Y. Chok, N.A. Nadhirah Azni, S. Santhiran, W. Shajahan, X.Y. Lai and V.R. Avupati, *Asian J. Chem.*, **36**, 1429 (2024); https://doi.org/10.14233/ajchem.2024.31558
12. T.T. Talele, P. Arora, S.S. Kulkarni, M.R. Patel, S. Singh, M. Chudayeu and N.K. Basu, *Bioorg. Med. Chem.*, **18**, 4630 (2010); https://doi.org/10.1016/j.bmc.2010.05.030
13. F.A. Saddique, M. Ahmad, U.A. Ashfaq, M. Muddassar, S. Sultan and M.E.A. Zaki, *Pharmaceuticals*, **15**, 106 (2022); https://doi.org/10.3390/ph15010106
14. S. Taj, M. Ahmad and U.A. Ashfaq, *Int. J. Biol. Macromol.*, **207**, 507 (2022); https://doi.org/10.1016/j.ijbiomac.2022.03.023
15. M. Madhuri, C. Prasad and V.R. Avupati, *Int. J. Comput. Appl.*, **95**, 13 (2014); https://doi.org/10.5120/16597-6403
16. B.K. Bugata, S.V.G.K. Kaladhar Dowluru and V.R. Avupati, *Int. J. Comput. Appl.*, **78**, 44 (2013); https://doi.org/10.5120/13587-1426
17. V.R. Avupati, R.P. Yejella, A. Akula, G.S. Guntuku, B.R. Doddi, V.R. Vutla, S.R. Anagani, L.S. Adimulam and A.K. Vyricharla, *Bioorg. Med. Chem. Lett.*, **22**, 6442 (2012); https://doi.org/10.1016/j.bmcl.2012.08.052
18. V. R. Avupati, P. N. Kurre, S. R. Bagadi, M. K. Muthyala and R. P. Yejella, *Chem-Bio Inform. J.*, **10**, 74 (2010); https://doi.org/10.1273/cbij.10.74
19. L. Sim, K. Jayakanthan, S. Mohan, R. Nasi, B.D. Johnston, B.M. Pinto and D.R. Rose, *Biochemistry*, **49**, 443 (2010); https://doi.org/10.1021/bi9016457
20. S.S. Elhady, N.M. Alshobaki, M.A. Elfaky, A.E. Koshak, M. Alharbi, R.F.A. Abdelhameed and K.M. Darwish, *Metabolites*, **13**, 942 (2023); https://doi.org/10.3390/metabo13080942
21. F.A. Saddique, S. Aslam, M. Ahmad, U.A. Ashfaq, M. Muddassar, S. Sultan, S. Taj, M. Hussain, D.S. Lee and M.E.A. Zaki, *Molecules*, **26**, 3043 (2021); https://doi.org/10.3390/molecules26103043
22. L.L. Landeros-Martínez, N. Gutiérrez-Méndez, J.P. Palomares-Báez, N.A. Sánchez-Bojorge, J.P.F.D.L. Ríos, H.A. Piñón-Castillo, M.A. Chávez-Rojo and L.M. Rodríguez-Valdez, *Appl. Sci.*, **11**, 4067 (2021); https://doi.org/10.3390/app11094067
23. A.L. Lovering, S.S. Lee, Y.-W. Kim, S.G. Withers and N.C.J. Strynadka, *J. Biol. Chem.*, **280**, 2105 (2005); https://doi.org/10.1074/jbc.M410468200
24. L. Zhang, X. Yin, H. Yang, H. Wen, S. Han, X. Pan, H. Li and D. Peng, *Foods*, **13**, 12 (2023); https://doi.org/10.3390/foods13010012